

## Dyons and Roberge - Weiss transition in lattice QCD

V. G. Bornyakov<sup>1,3,a</sup>, D. L. Boyda<sup>1,2,4</sup>, V. A. Goy<sup>1,2,4</sup>, E.-M. Ilgenfritz<sup>5</sup>, B. V. Martemyanov<sup>4</sup>, A. V. Molochkov<sup>1,4</sup>, Atsushi Nakamura<sup>1,6,7</sup>, A. A. Nikolaev<sup>1,4</sup>, and V. I. Zakharov<sup>1,4</sup>

<sup>1</sup>*School of Biomedicine, Far Eastern Federal University, 690950 Vladivostok, Russia*

<sup>2</sup>*School of Natural Sciences, Far Eastern Federal University, 690950 Vladivostok, Russia*

<sup>3</sup>*Institute for High Energy Physics NRC Kurchatov Institute, 142281 Protvino, Russia,*

<sup>4</sup>*Institute of Theoretical and Experimental Physics NRC Kurchatov Institute, 117218 Moscow, Russia*

<sup>5</sup>*Joint Institute for Nuclear Research, BLTP, 141980 Dubna, Russia*

<sup>6</sup>*Research Center for Nuclear Physics (RCNP), Osaka University, Ibaraki, Osaka, 567-0047, Japan,*

<sup>7</sup>*Theoretical Research Division, Nishina Center, RIKEN, Wako 351-0198, Japan*

**Abstract.** We study lattice QCD with  $N_f = 2$  Wilson fermions at nonzero imaginary chemical potential and nonzero temperature. We relate the Roberge - Weiss phase transition to the properties of dyons which are constituents of the KvBLL calorons. We present numerical evidence that the characteristic features of the spectral gap of the overlap Dirac operator as function of an angle modifying the boundary condition are determined by the  $Z_3$  sector of the respective imaginary chemical potential. We then demonstrate that dyon excitations in thermal configurations could be responsible (in line with perturbative excitations) for these phenomena.

### 1 Introduction

Confinement (of quarks and gluons) and spontaneous breaking of chiral symmetry at low temperature and density are two basic properties of QCD. These properties are connected with each other and originate from the complex structure of the QCD vacuum state. The latter is reflected, for example, in the condensates of gluon and quark fields. These condensates (as vacuum expectation values) are of course space and time independent but field fluctuations contributing to them are both space-time and scale dependent. Considerable activity in Lattice Gauge Theory has the aim to reveal the corresponding structures. Semiclassical objects of QCD are since long particular candidates to form these structures at the infrared scale. The density and internal characteristics of semiclassical objects could depend on external conditions (temperature, density etc.) thus providing (or at least assisting) different phase transitions.

For long time it is known that the instanton mechanism is able to explain chiral symmetry breaking while it was impossible to construct an instanton mechanism for confinement in terms of an instanton gas or liquid, which are simple realizations of a multi-instanton-antiinstanton system. Specific constituent dyons of Kraan-van Baal-Lee-Lu (KvBLL) calorons [1–3] (with twist), however, can – in the same way as instantons – explain chiral symmetry breaking. But calorons with their dyon “substructure” are able also to reproduce different features of confinement (Polyakov loop correlators, spatial

<sup>a</sup>e-mail: vitaly.bornyakov@ihep.ru

string tension, vortex and/or monopole percolation). All this has added qualitative arguments to the expectations already existing for decades that “instanton quarks” (carriers of fractional topological charge) might solve the confinement problem. Moreover, dyons when considered as rarefied gas (in three dimensions), either without interaction or with some kind of Coulomb-like interaction, give confining behavior for space-like Wilson loops and for correlators of Polyakov loops. This idea has been developed from the 70’s to the recent past [4–8].

The modelling of dyon ensembles with interaction has attracted more attention recently [9–15]. Therefore, it was important before as it is important now to identify dyons in thermal lattice configurations (from quenched simulations or from full QCD with dynamical fermions) which are thought to represent lattice gauge fields at different temperatures and possibly further external parameters). The aim is to assess the relevance of these models and in particular to clarify the importance of dyon degrees of freedom.

The caloron with nontrivial holonomy [1–3] has the remarkable property that the single zero mode of the Dirac operator is located only on the “twisted” (Kaluza-Klein) dyon constituent when standard antiperiodic boundary conditions are applied to the Dirac spectrum. Depending on different temporal boundary condition (b.c.) applied to the Dirac operator (with improved chiral properties), this zero mode may delocalize and localize again on distinct constituent dyons [16, 17]. Under certain circumstances these dyons can appear as distinct entities, but the fractional topological charge  $1/N_c$  is only realized in the case of “maximally nontrivial holonomy”, *i.e.* in the confinement phase.

For definiteness, inspecting thermal lattice configurations of fixed total topological charge  $Q = \pm 1$  (below and above  $T_c$ ) such a change of the single zero mode’s location with the change of b.c. was initially observed in [18, 19] and interpreted according to the caloron picture taking care of the unit topological charge.

This property of mobility (and a changing degree of localization) is shared also by a band of near-zero modes of the overlap Dirac operator as was shown by some of the present authors in a series of papers [20–23].

In this paper we use the above properties of calorons and of their constituent dyons in order to investigate the question whether dyons can contribute to the Roberge-Weiss (RW) phase transitions, which themselves are an outstanding feature of simulations at imaginary chemical potential.

Imaginary chemical potential is not hampered by the sign problem which, on the other side, prohibits direct grand canonical simulations with real baryonic chemical potential. Therefore standard Hybrid Monte Carlo algorithms can be applied to simulate lattice QCD in this extension of the case  $\mu = 0$ . For our investigation we employ dynamical QCD configurations primarily generated at imaginary chemical potential as part of a project aiming to study finite baryonic density within the canonical approach.

It is appropriate to remind the reader that there have been two reasons to propose a detour to imaginary chemical potential, both with the final aim to obtain (grand canonical or canonical) results for finite baryonic density (see *e.g.* the review paper [24]).

The first step in both strategies are grand canonical simulations at imaginary chemical potential. The respective ideas are

- analytical continuation of observables considered as functions of imaginary  $\mu = i\mu_I$  to real  $\mu$ ;
- the “measurement” of the grand canonical partition function as function of imaginary chemical potential. The aim in the second case is to make it possible to perform the Fourier transformation with respect to  $\mu_I$  in order to get the partition function for fixed baryon number  $B$  in the system (canonical approach).

These ideas have motivated the study of lattice QCD at imaginary chemical potential in a broader sense than restricted to the two purposes. The study of the phase transitions there (in particular the

Roberge-Weiss transition to be mentioned next) is important since their properties can be related to properties of the phase transition in thermal QCD at zero chemical potential (see *e.g.* [25] and references therein).

Here we only briefly notice some basic facts of simulations with imaginary chemical potential  $\mu_q = i\mu_I$  which are important for our aim. It is convenient to introduce an angle  $\theta = \mu_I/T$ . Then the QCD partition function at temperature  $T$  is a periodic function of  $\theta$ :

$$Z(T, \theta) = Z(T, \theta + 2\pi/N_c). \quad (1)$$

$N_c$  is the number of colors, in our case  $N_c = 3$ . This periodicity property is called Roberge-Weiss symmetry [26]. QCD possesses a rich phase structure at nonzero  $\theta$ , which depends on the number of flavors  $N_f$  and the quark masses  $m_q$  (or a single quark mass in the case of  $N_f = 2$ ). The phase structure for  $N_f = 2$  and intermediate quark mass is schematically shown in Fig. 1.

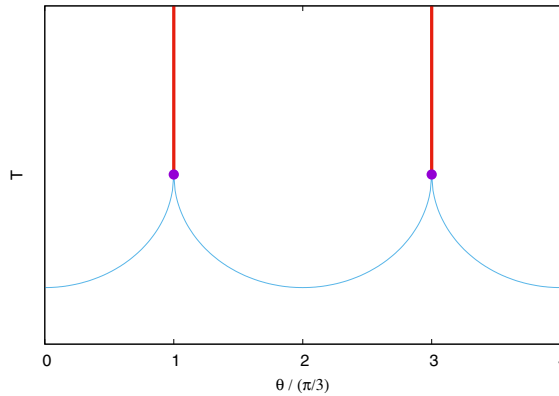


**Figure 1.** Phase diagram of QCD in the temperature–imaginary chemical potential ( $\theta = \mu_I/T$ ) plane for intermediate quark masses. Thick vertical lines denote first order RW transitions, thin curly lines denote crossover lines, and thick points mark second order transition points, where a line of first order transition ends.

There are first order phase transitions at  $\theta = (2k + 1)\pi/3$  for temperatures  $T > T_{RW}$  [26] where  $T_{RW}$  is somewhat higher than  $T_c$  - the temperature of the crossover to the quark-gluon plasma phase at zero chemical potential. These transitions are shown as thick vertical lines in Fig. 1. These are transitions between  $Z(3)$  sectors of the theory. A particular sector can be identified by the phase of the average Polyakov loop. In Fig. 2 we show a scatter plot for the volume-averaged Polyakov loop  $PL$  computed for different values of  $\theta$ . The Polyakov loop has been computed for  $\theta$  from 0 to  $\pi$ . For other values of  $\theta$  its values were obtained using the fact that  $\text{Im}(PL)$  ( $\text{Re}(PL)$ ) is an odd (an even) function of  $\theta$ . One can see all three patches corresponding to the three  $Z_3$  sectors.

We have also checked that the values of  $PL$  in one  $Z_3$  sector can be obtained by respective center transformation from its values in another another  $Z_3$  sector:  $PL(\theta + 2k\pi/3) = G_k PL(\theta)$  where  $G_k$  denotes rotation by  $2k\pi/3$  in the  $PL$  complex number plane.

The important role of dyons in the Roberge-Weiss transition, that we are going to demonstrate, also underlines their importance for QCD in general. To our best knowledge this is a first study of

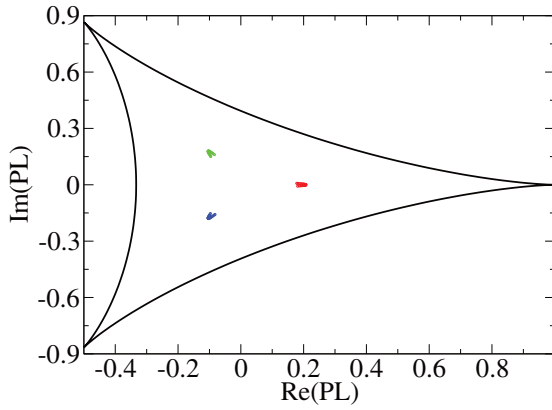


**Figure 2.** Scatter plot for Polyakov loop  $PL$  at  $T = 1.35T_c > T_{RW}$  with variation of  $\theta = \mu_I/T$  inside the three basic intervals  $[-\pi/3, \pi/3]$ ,  $[\pi/3, \pi]$ , and  $[\pi, 5\pi/3]$  corresponding to the three  $Z_3$  sectors.

the role of nonperturbative fluctuations within thermal QCD at imaginary chemical potential. We will present evidence that the dyons could (together with perturbative fluctuations) contribute to the transitions and thus influence the strength of the RW transitions. Our argument is as follows. It is evident that low modes of the quark determinant (at least for small dynamical quark masses) play a crucial role in the resulting phase structure depicted in Fig. 1. It is then important to identify the fluctuations responsible for the low modes. We will present numerical evidence supporting idea that dyons are such fluctuations.

In Section 2 we introduce the lattice set-up in which the ensembles of gauge fields, that we are going to analyze have been generated in lattice QCD with  $N_f = 2$  dynamical flavors and imaginary chemical potential. We also define all the topologically relevant lattice observables employed later on for the analysis.

Then, in Section 3 we present results on the spectrum. Namely, we show the gap in the spectrum as a function of an angle in the fermionic temporal boundary conditions for some representative configurations generated with different imaginary chemical potentials. Also as a counter example we show such a gap for one configuration for  $T < T_c$ .

We also show gap results for artificially created configurations including pairs of dyons and anti-dyons and argue that they have similar properties and contribute to the partition function in such a way as to increase the strength of the RW transition. In Section 4 we shall draw our conclusions.

## 2 Lattice Setting for the Thermal Ensembles

We study lattice QCD with  $N_f = 2$  light quarks using the clover improved Wilson action defined by the fermion matrix

$$\begin{aligned} \Delta(n, m, \mu_q) &= \delta_{nm} - \kappa C_{SW} \delta_{nm} \sum_{\mu \leq \nu} \sigma_{\mu\nu} F_{\mu\nu} - \kappa \sum_{i=1}^3 \left[ (1 - \gamma_i) U_i(n) \delta_{m, n+\hat{i}} + (1 + \gamma_i) U_i^\dagger(m) \delta_{m, n-\hat{i}} \right] \\ &- \kappa \left[ e^{+\mu_q a} (1 - \gamma_4) U_4(n) \delta_{m, n+\hat{4}} + e^{-\mu_q a} (1 + \gamma_4) U_4^\dagger(m) \delta_{m, n-\hat{4}} \right] \equiv 1 - \kappa Q(\mu_q). \end{aligned} \quad (2)$$

where  $\kappa$  is the hopping parameter and  $c_{SW}$  - the improvement coefficient. For the gluon field we adopt the Iwasaki improved gauge field action

$$S_g = \frac{\beta}{6} \left[ c_0 \sum_{n,\mu<\nu} W_{\mu\nu}^{1\times 1}(n) + c_1 \sum_{n,\mu<\nu} W_{\mu\nu}^{1\times 2}(n) \right] \quad (3)$$

where  $c_1 = -0.331$  and  $c_0 = 1 - 8c_1$ . We generate configurations on  $16^3 \times 4$  lattices at  $\beta = 2.0$ ,  $\kappa = 0.136931$  and  $c_{SW} = (1 - 0.8412\beta^{-1})^{-3/4}$ . These parameters correspond to a temperature ratio  $T/T_c = 1.35$  for a quark mass determined by a target mass ratio  $m_\pi/m_\rho = 0.8$ . All parameters of the action including  $c_{SW}$  value were borrowed from the WHOT-QCD collaboration paper [27].

The overlap Dirac operator  $D$  fulfills the Ginsparg-Wilson equation [28]. A possible solution – for any *input Dirac operator*, in our case for the mostly used Wilson-Dirac operator  $D_W$  – is the following zero-mass overlap Dirac operator [29, 30]

$$D(m=0) = \frac{\rho}{a} \left( 1 + \frac{D_W}{\sqrt{D_W^\dagger D_W}} \right) = \frac{\rho}{a} (1 + \text{sgn}(D_W)) , \quad (4)$$

with  $D_W = M - \rho/a$ , where  $M$  is the hopping term of the Wilson-Dirac operator and  $\rho/a$  is a negative mass term usually determined by optimization. The index of  $D$ , i. e. the difference of its number of right-handed and left-handed zero modes  $\psi_0$  with chirality  $\pm 1$ , can be identified with the integer-valued topological charge  $Q_{\text{over}}$  [31]. The non-zero modes appear in pairs, which are related to each other by  $\psi_\lambda = \gamma_5 \psi_{-\lambda}$ , and have vanishing chirality.

The diagonalization of the overlap operator is achieved using a variant of the Arnoldi algorithm [32]. We have computed 20 lowest eigenmodes.

We consider generalized boundary conditions for any Dirac operator underlying the diagonalization

$$\psi(\vec{x}, x_4 + \beta) = \exp(i\phi) \psi(\vec{x}, x_4) . \quad (5)$$

While the physical fermion sea is described by the clover-improved Wilson-Dirac operator, implemented with antiperiodic temporal boundary conditions ( $\phi = \pi$ ), the introduction of the imaginary chemical potential is equivalent to subjecting the Dirac operator for physical fermions to continuously modified temporal boundary conditions characterized by the angle  $\theta = \mu_I/T$ ,

$$\psi(\vec{x}, x_4 + \beta) = \exp(i(\pi - \theta)) \psi(\vec{x}, x_4) . \quad (6)$$

The following values of  $\phi$

$$\phi = \left\{ \begin{array}{c} -\pi/3 \\ +\pi/3 \\ \pi \end{array} \right\} \quad (7)$$

correspond to elements in the boundary condition for which on a single caloron solution the corresponding fermion zero modes become maximally localized at one of its three constituent dyons. Note that  $\phi_3$  corresponds to the antiperiodic boundary condition.

### 3 Results for the spectral gap

In our study of the low modes we use the (massless) overlap lattice Dirac operator rather than the clover-improved Wilson-Dirac operator for which gauge field configurations had been simulated. This

is partially due to the fact that it would have exact zero modes on topologically nontrivial configurations which helps the safe discrimination between zero and nonzero modes and makes possible the unambiguous introduction of the gap into the consideration. For brevity we will call it simply "the Dirac operator".

In Fig. 3 we show the spectra of the Dirac operator for two configurations. Configuration I (left part) was generated at  $\theta_I = 1 < \pi/3$  ( $\phi_I = -1 + \pi$ ), while configuration II (right part) - at  $\theta_{II} = 1.1 > \pi/3$  ( $\phi_{II} = -1.1 + \pi$ ). The configurations are taken from ensembles lying on both sides of the first Roberge-Weiss transition value  $\theta = \pi/3$ . When we change the phase  $\phi$  in the overlap Dirac operator to be diagonalized for configuration I from  $\phi_1 = \phi_I$  to  $\phi_2 = 0.24 \cdot (2\pi) < \phi_{II}$ , we find the spectrum changing in the left part of the figure from blue circles to red upside triangles. We see that even a small change of  $\phi$  across the phase transition (corresponding to the displacement to the "wrong" phase) gives rise to a drastic change of the spectrum: the eigenvalues are shifted to smaller values thus decreasing the gap. It is evident that this change of the spectrum implies a substantial decreasing of the Dirac operator determinant thus indicating that the statistical weight of configuration I displaced to the region  $\theta > \pi/3$  is small.

We make a similar observation for the configuration II after changing the phase  $\phi$  in the overlap Dirac operator from  $\phi_2 = \phi_{II}$  to  $\phi_1 = 0.422 \cdot (2\pi) > (-\theta_I + \pi)$ . The respective spectra undergo similar changes (shown in the right panel) and thus configuration II would acquire a small statistical weight for  $\theta < \pi/3$ .

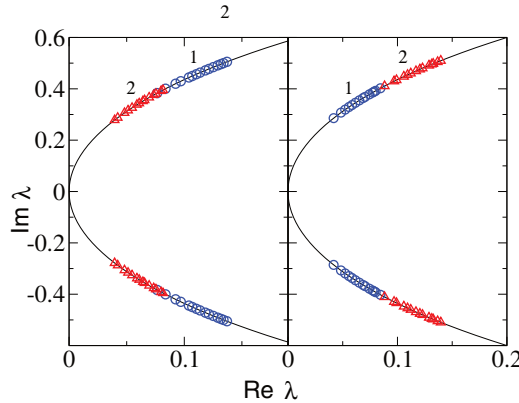


**Figure 3.** Spectra of the overlap Dirac operator for two configurations. Left panel: two spectra for configuration I. Spectrum 1 is for an angle  $\phi$  in the overlap Dirac operator boundary condition  $\phi_1 = \phi_I$ , spectrum 2 - for  $\phi_2 = 0.24 \cdot (2\pi) < (-\theta_{II} + \pi)$ . Right panel: two spectra for configuration II. Spectrum 2 is for an angle  $\phi$  in the overlap Dirac operator's boundary condition  $\phi_2 = \phi_{II}$ , spectrum 1 - for  $\phi_1 = 0.422 \cdot (2\pi) > (-\theta_I + \pi)$ .

We then are going to measure the spectrum for these two configurations I and II) for a few values of  $\phi$  in the Dirac operator boundary condition in order to cover the range of  $\phi$  between 0 and  $2\pi$ . Additionally, we do the same for a configuration III generated at  $\theta_{III} = 3.2 > \pi$ , i.e. beyond the second Roberge-Weiss transition, in other words, in the third  $Z_3$  sector.

In Fig. 4 we show the spectral gap as a function of  $\phi$  for configurations I (red solid lines), II (blue dashed line) and III (green dotted line), representing all three center sectors. The points on these curves marked with symbols correspond to the value of  $\theta$  used in the generation of the corresponding configurations. Such a dependence of the gap on the angle in the fermionic boundary condition is

already known for different thermal configurations of SU(3) Yang-Mills theory and QCD at zero chemical potential [33] but the origin of the dependence was not discussed there.

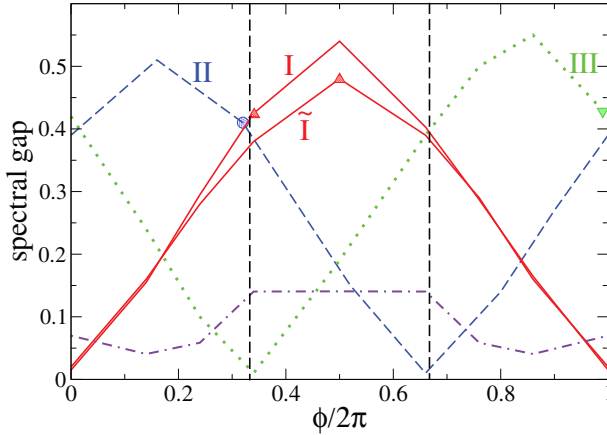


**Figure 4.** Spectral gap of the overlap Dirac operator as function of  $\phi$  for four thermal configurations (two red solid curves, one dashed blue curve and one green dotted curve) generated at  $T = 1.35T_c$  and for one further thermal configuration (one violet dash-dotted curve) generated at  $T < T_c$ . See explanations in the text.

We see from this figure that configuration I (generated at  $\phi \in [2\pi/3; 4\pi/3]$ ) has a maximal gap (and thus a maximal weight) among three configurations I, II, III in the range of  $\phi$  between (approximately)  $2\pi/3$  and  $4\pi/3$ . Configuration II (generated at  $\phi \in [0; 2\pi/3]$ ) has a maximal gap in the range from 0 to  $2\pi/3$ , and configuration III (generated at  $\phi \in [4\pi/3; 2\pi]$ ) has a maximal gap in the range from  $4\pi/3$  to  $2\pi$ .

Thus we observe that the Roberge-Weiss transition is accompanied by the drastic change in the gauge field configurations: configurations generated on one side of the transition have small statistical weight on the other side of it due to drastic change in respective Dirac operator spectrum.

In Fig. 4 we additionally show the spectral gap for one more configuration  $\tilde{I}$  from the first Roberge-Weiss sector but generated at zero imaginary chemical potential  $\theta = 0$ . One can see that the spectral gaps for two configurations generated at two different values of  $\theta$  from the same Roberge-Weiss sector are qualitatively very similar. Thus we may extend conclusions about the spectral gaps of the configurations I - III to all configurations of all three Roberge-Weiss sectors.

It is important to clarify what fluctuations of the gauge field are responsible for these properties of the Dirac operator spectrum.

Let us now consider the Dirac operator spectrum in the background of an artificially created configuration. Such configuration was considered in [23], details of its construction can be found in that paper. The three dyons of a given caloron have different actions determined by the asymptotic holonomy. For the holonomy approaching one of  $Z_3$  center element there are two light dyons and one heavy dyon. We start from a caloron-anticaloron configuration and remove the heavy dyon and the heavy antidyon. Thus, our configuration consists of two light dyons and two light antidyons, see eq. (36) and eq. (37) of Ref. [23].

In [23] we have presented numerical evidence that dyons of the heavy type are rare in the deconfining phase of lattice QCD with zero chemical potential.

It is known that for a caloron configuration the zero mode of the Dirac operator is localized on one of the dyons depending on boundary conditions (or equivalently, on the holonomy). This is also true for near zero modes. For a heavy dyon-antidyon pair the near-zero modes appear when holonomy is close to  $Z_3 = I$  and  $\phi = \pi$  (antiperiodic boundary conditions), see the right-most panel of Fig. 1 in Ref. [23]. In distinction to that, when we consider a configuration without heavy (anti)dyons, e.g. a configuration consisting of a light double dyon - antidyon pair we find rather large gap in the spectrum, see the right-most panel of Fig. 4 in Ref. [23]. In [23] we have presented numerical evidence that in the deconfinement phase of lattice SU(3) gluodynamics heavy dyons are suppressed and low modes in the spectrum of thermal configurations are resembling the spectrum of the artificial configuration with light double dyon - antidyon pair.

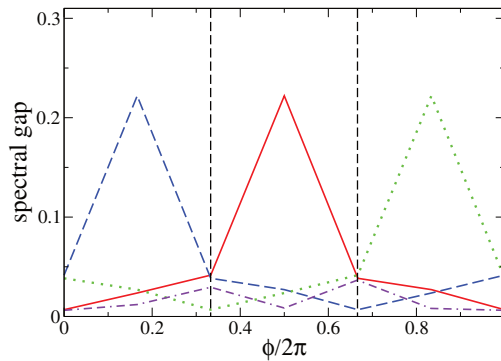


**Figure 5.** Spectral gap of the overlap Dirac operator for three artificial configuration as function of  $\phi$ . See explanations in the text.

In Fig. 5 we show the spectral gap for the configuration with a light double dyon - antidyon pair as function of  $\phi$ . We see that the dependence of the gap on  $\phi$  is qualitatively the same as that of thermal configurations from the  $Z_3 = I$  Roberge-Weiss sector (red solid curve in Fig. 4): the maximum is at  $\phi = \pi$  and the gap decreases to a minimal value (which is rather close to zero) at  $\phi = 0$  or  $\phi = 2\pi$ . For artificial configurations that differ from this one by center transformations  $Z_3 = e^{i2\pi/3}$  or  $Z_3 = e^{i4\pi/3}$  light and heavy dyons simply change their enumeration

$$1 \rightarrow 2, 2 \rightarrow 3, 3 \rightarrow 1$$

or

$$1 \rightarrow 3, 3 \rightarrow 2, 2 \rightarrow 1$$

(see the corresponding blue dashed and green dotted curves).

Results obtained for the spectral gap for these artificial dyon configurations demonstrate that such configurations allow to explain the main characteristic features of the spectral gap obtained for equilibrium configurations shown in Fig. 4. It is important to notice that the results for artificial caloron-anticaloron configuration (all three dyons and antidyons present, represented by the violet dash-dotted curve in Fig. 5) are qualitatively different from the results for the artificial dyon configuration: the

spectral gap practically (compared to the other curves in Fig. 5) does not depend on the boundary condition. In this respect these results are similar to the results of Fig. 4 where the gap for a configuration from the confining phase (violet dash-dotted curve) has the same property.

## 4 Conclusions

We made a study of the low modes spectrum of the overlap Dirac operator lattice QCD with  $N_f = 2$  flavors of clover-improved Wilson fermions at  $T/T_c = 1.35$  and  $T/T_c < 1$  (with  $m_\pi/m_\rho = 0.8$ ) at nonzero imaginary chemical potential. We have considered equilibrium configurations generated at particular values of the imaginary chemical potential taken from all three Roberge-Weiss (center) sectors. We have computed 20 lowest modes of the Dirac operator for every such configuration varying the imaginary chemical potential in the analysing Dirac operator.

We observed (see Fig. 4) that the spectral gap has some uniform characteristic features for equilibrium configuration generated at non-vanishing imaginary chemical potential  $\theta$  anywhere in the given Roberge-Weiss (center) sector.

- This gap (as a function of an angle in the boundary condition for the analysing overlap Dirac operator) has a maximum in the middle of the Roberge-Weiss sector and decreases monotonously;
- this behavior is independent of the particular value of  $\theta$  inside the sector where the configuration has been generated.
- The spectral gaps for two sectors intersect at the boundary between them. This means that configurations generated at  $\theta$  from one sector have low statistical weight in another sector.

We have argued that the reason for such behavior of the spectral gap could be partially connected to nonperturbative objects present in equilibrium configuration, constituent dyons of calorons.

## Acknowledgments

The authors are grateful to Ph. de Forcrand for useful remarks. The work was completed due to support of the Russian Science Foundation via grant number 15-12-20008. Computer simulations were performed on the FEFU GPU cluster Vostok-1 and MSU 'Lomonosov' supercomputer.

## References

- [1] T. C. Kraan and P. van Baal, Nucl.Phys. **B533**, 627 (1998), hep-th/9805168.
- [2] T. C. Kraan and P. van Baal, Phys.Lett. **B435**, 389 (1998), hep-th/9806034.
- [3] K.-M. Lee and C.-H. Lu, Phys.Rev. **D58**, 025011 (1998), hep-th/9802108.
- [4] A. M. Polyakov, Nucl. Phys. **B120**, 429 (1977).
- [5] B. Martemyanov and S. Molodtsov, JETP Lett. **65**, 142 (1997).
- [6] P. Gerhold, E.-M. Ilgenfritz, and M. Müller-Preussker, Nucl. Phys. **B760**, 1 (2007), hep-ph/0607315.
- [7] D. Diakonov and V. Petrov, Phys.Rev. **D76**, 056001 (2007), 0704.3181.
- [8] F. Bruckmann, S. Dinter, E.-M. Ilgenfritz, B. Maier, M. Müller-Preussker, and M. Wagner, Phys.Rev. **D85**, 034502 (2012), 1111.3158.
- [9] E. Shuryak, J. Phys. **G39**, 054001 (2012), 1112.2573.
- [10] P. Faccioli and E. Shuryak, Phys. Rev. **D87**, 074009 (2013), 1301.2523.
- [11] R. Larsen and E. Shuryak (2014), 1408.6563.
- [12] Y. Liu, E. Shuryak, and I. Zahed (2015), 1503.03058.
- [13] Y. Liu, E. Shuryak, and I. Zahed (2015), 1503.09148.

- [14] R. Larsen and E. Shuryak (2015), 1504.03341.
- [15] Y. Liu, E. Shuryak and I. Zahed, arXiv:1606.07009 [hep-ph].
- [16] M. Garcia Perez, A. Gonzalez-Arroyo, C. Pena, and P. van Baal, Phys.Rev. **D60**, 031901 (1999), hep-th/9905016.
- [17] M. N. Chernodub, T. C. Kraan, and P. van Baal, Nucl. Phys. Proc. Suppl. **83**, 556 (2000), hep-lat/9907001.
- [18] C. Gattringer, Phys. Rev. **D67**, 034507 (2003), hep-lat/0210001.
- [19] C. Gattringer and S. Schaefer, Nucl. Phys. **B654**, 30 (2003), hep-lat/0212029.
- [20] V. Bornyakov, E.-M. Ilgenfritz, B. Martemyanov, S. Morozov, M. Müller-Preussker, and A. Veselov, Phys.Rev. **D76**, 054505 (2007), 0706.4206.
- [21] V. Bornyakov, E.-M. Ilgenfritz, B. Martemyanov, and M. Müller-Preussker, Phys.Rev. **D79**, 034506 (2009), 0809.2142.
- [22] E.-M. Ilgenfritz, B. Martemyanov, and M. Müller-Preussker, Phys.Rev. **D89**, 054503 (2014), 1309.7850.
- [23] V. G. Bornyakov, E. M. Ilgenfritz, B. V. Martemyanov, and M. Muller-Preussker, Phys. Rev. **D91**, 074505 (2015), 1410.4632.
- [24] S. Muroya, A. Nakamura, C. Nonaka, and T. Takaishi, Prog. Theor. Phys. **110**, 615 (2003), hep-lat/0306031.
- [25] C. Bonati, P. de Forcrand, M. D'Elia, O. Philipsen, and F. Sanfilippo, Phys. Rev. **D90**, 074030 (2014), 1408.5086.
- [26] A. Roberge and N. Weiss, Nucl. Phys. **B275**, 734 (1986).
- [27] S. Ejiri, Y. Maezawa, N. Ukita, S. Aoki, T. Hatsuda, N. Ishii, K. Kanaya, and T. Umeda (WHOT-QCD), Phys. Rev. **D82**, 014508 (2010), 0909.2121.
- [28] P. H. Ginsparg and K. G. Wilson, Phys. Rev. **D25**, 2649 (1982).
- [29] H. Neuberger, Phys. Lett. **B417**, 141 (1998), hep-lat/9707022.
- [30] H. Neuberger, Phys. Lett. **B427**, 353 (1998), hep-lat/9801031.
- [31] P. Hasenfratz, V. Laliena, and F. Niedermayer, Phys. Lett. **B427**, 125 (1998), hep-lat/9801021.
- [32] H. Neff, N. Eicker, T. Lippert, J. W. Negele and K. Schilling, Phys. Rev. D **64**, 114509 (2001) doi:10.1103/PhysRevD.64.114509 [hep-lat/0106016].
- [33] E. Bilgici et al. (2009), 0906.3957.